AIAA JOURNAL
Vol. 38, No. 1, January 2000

# Impedance and Its Time-Domain Extensions

K.-Y. Fung* and Hongbin Ju†
*Hong Kong Polytechnic University, Kowloon, Hong Kong, People's Republic of China*
and
BhanuPrakash Tallapragada‡
*Andhra University, Visakhapatnam 530 003, India*

**The classical concept of impedance as a means to characterize the reflectivity and absorption of a surface to the incident waves has always been a complex-valued quantity akin to plane harmonic waves and the analysis of their reflections. A new look at this classical quantity irrespective of the type of incident waves is presented. It points out that a direct operational inversion of impedance into time-domain boundary operators will, in general, lead to an unstable system, whereas the inversion of the corresponding reflection coefficient will result in stable, easily implementable boundary operators for time-domain prediction of wave reflection. It reveals the equivalent, pulselike, causal process of time convoluting the incident wave into the reflected wave. Excellent agreement with analytical solutions derived here and from other sources supports the validity of the approach and demonstrates the accuracy of the implementations.**

## Introduction

THE reflection of waves from walls other than those with a simple smooth surface can be the result of rather complex processes, which ordinarily are not of immediate interest to the observer. The resulting reflections observed at distances are the subject of many studies and applications. The classical model is to characterize the reflective surface according to the concept of impedance $Z$ that relates a surface pressure harmonic component $\hat{p}$ to the corresponding rate of deformation, or normal velocity $\hat{u}_n$, of the reflecting surface, that is, $\hat{p} = Z(\omega, \theta)\hat{u}_n$. Here the caret denotes Fourier components, $\omega$ denotes the circular frequency, and $\theta$ denotes the incident angle. Time dependence $e^{i\omega t}$ is assumed. Often, the locally reactive assumption that $Z$ depends only on frequency is made for simplicity and practicality. The determination of this complex-valued constant requires both accurate measurement and prediction techniques, which have been the subjects of continuing studies since 1914 (Ref. 1). The concept itself, as well as all measurement techniques, is based on the reflection of plane harmonic waves. The majority of experiments are restricted to two classes, the impedance tube and the reflection of harmonic sources. With an acoustic source placed at one end of the impedance tube and the tested material at the other, impedance is determined by comparison with the solution of one-dimensional harmonic standing waves. This simple method is known to be restrictive in frequency range, sensitive to mounting conditions, and appropriate for testing locally reactive materials only. The recent work of Jones and Stiede[2] compares the strengths and weaknesses of various implementations of this rather old technique for further improvement. The measurement of the reflection of a source from an impedance plane poses little problem for modern data acquisition systems, except for the consideration of controlling the testing conditions of large spaces. Unfortunately, the general solution of the reflection of the sound field above an impedance plane due to a point source is not amenable to easy computation.[3] The difficulty is due to having to convert spherical waves into plane harmonic waves for which impedance is defined. Nonetheless, various asymptotically expanded formulas in terms of a distance parameter formed by horizontal distance, wave number, and impedance have been proposed[4–6] and used as the bases for various measurement techniques in field and in situ determination of impedance.[7–9] They are, however, restrictive in application distance, range of frequency, and type of source. Had a general method valid for close range between the source and the wall regardless of the value of impedance been available, these field and in situ techniques would have gained much wider acceptance.

The most serious drawback in the development of methods for analysis and experimentation is the assumption of plane harmonic waves, which requires larger testing spaces for lower frequencies to avoid contamination. Many of the aforementioned methods are, therefore, restricted to locally reactive impedances at high frequencies. In principle, the reflective condition of a wall is defined by a measure of the reflected wave. A finite time history of the reflected wave measured on any hemispherical surface centered about the point of normal incidence should contain the same information about the reflective wall regardless of the radius of the hemisphere. Unfortunately, such a time-domain prediction method, or reference solution, with the incorporation of corresponding boundary conditions for general values of $Z$, has not been established or found in the open literature.

The corresponding theory for imposing a time-domain impedance condition has been of little interest to researchers until the recent development of time-domain methods for waves.[10–14] A straightforward application of operational mathematics would suggest the expansion of $Z(\omega)$ in powers of $(i\omega)^k$ and conversion into corresponding operators $(\mathrm{d}^k/\mathrm{d}t^k)$. Davis[10] attempted an equivalent time-domain impedance condition for the reflection of acoustic waves at the open end of a pipe, but did not demonstrate the stability of his implementation. Yee et al.[15] constructed a stable time-domain operator for positive reactance. Lee et al.[16] modeled the impedance by a rational function and constructed the corresponding time-domain partial differential equation for the boundary points. Fang and Xeu[17] applied the impedance condition to the Fourier transform of the time-domain solution for the reflection of microwaves and proposed a correction factor for phase error due to the difference scheme used. Tam and Auriault[18] constructed stable impedance-dependent schemes for the reflection of single- and banded-frequency acoustic waves. Özyörük et al.[19] devised time-domain impedance operators via the $z$ transform and applied their method to predict the decay of waves in a flow impedance tube.

It will be shown that a direct inversion of $Z(\omega)$ generally results in an unstable system of temporal operators. If, instead, the equivalent temporal system is derived from the corresponding reflection coefficient $\hat{W}(\omega)$, its stability and convergence are ensured. This

Received 9 December 1998; revision received 4 June 1999; accepted for publication 9 June 1999. 

*Professor, Department of Mechanical Engineering, Hung Hom. Associate Fellow AIAA.

†Postdoctoral Fellow, Department of Mechanical Engineering, Hung Hom; permanent address: School of Power and Energy Engineering, Shanghai Jiao Tong University, 200030 Shanghai, People's Republic of China.

‡Assistant Professor, Department of Marine Engineering.

concept is further extended into a direct time-domain equivalent of impedance. Implementation issues will be discussed, and benchmarking solutions in one and two dimensions are given.

## Impedance Condition

Let $u(x, t)$ and $p(x, t)$ be, respectively, the velocity and sound pressure nondimensionalized by the length $L$, sound speed $C$, time $L/C$, density $\rho$, and the dynamic pressure $\rho C^2$ satisfying the coupled wave system

$$\frac{\partial}{\partial t}\begin{bmatrix} u \\ p \end{bmatrix} + \begin{bmatrix} 0 & 1 \\ 1 & 0 \end{bmatrix}\frac{\partial}{\partial x}\begin{bmatrix} u \\ p \end{bmatrix} = \begin{bmatrix} 0 \\ 0 \end{bmatrix} \tag{1}$$

and let $u^+(x - t)$ and $u^-(x + t)$ be the uncoupled forward- and backward-propagating simple waves through the linear relation

$$\begin{bmatrix} u^+ \\ u^- \end{bmatrix} = \begin{bmatrix} 1 & 1 \\ 1 & -1 \end{bmatrix}\begin{bmatrix} u \\ p \end{bmatrix} \tag{2}$$

Regardless of the scheme used for solving Eq. (1), $u^+$ at a right boundary and $u^-$ at a left boundary, respectively, where they exit, must not be affected by the implementation of any boundary condition, the principle of causality, or the domain of dependence. Their values at the corresponding boundaries for a future time can, however, be obtained from the current spatial distribution by the method of characteristics and, hence, are given or available at all times. The Fourier transforms $\hat{u}$ and $\hat{p}$ must then satisfy the relation $\hat{u} + \hat{p} = \hat{u}^+$ or

$$[1 + Z(\omega)]\hat{u} = \hat{u}^+ \tag{3}$$

by the introduction of the impedance condition $\hat{p} = Z\hat{u}$. The solution of Eq. (3) in the frequency domain is straightforward, but the corresponding differential system is unstable unless all roots of $[1 + Z(\omega)]$ in the range of interest have positive imaginary parts, which generally cannot be assumed.

To wit, let the real and imaginary parts $R$ and $X$ of $Z$ be expanded in even and odd powers, respectively, of $\omega$ in the form

$$Z(\omega) = R + iX = R_0 + R_2\omega^2 + \cdots + i(X_1\omega + X_3\omega^3 + \cdots) \tag{4}$$

It should be noted that $Z$ itself is a simplified model and may assume any form of expansion as long as the range of values of interest is covered. Examine the simplest case where all coefficients are zero except $X_1$ and $u$ has the single frequency $\Omega$, a fixed value that may differ from and not be treated as the Fourier variable $\omega$. The equivalent time-domain impedance condition

$$\left[1 + X_1\frac{\mathrm{d}}{\mathrm{d}t}\right]u = u^+$$

has the homogeneous solution $\exp(-t/X_1)$ and is unstable for negative $X_1$. However, by first dividing Eq. (3) by $iX_1\Omega$, a stable system for negative $X_1$ can be chosen, that is,

$$\left[1 - \frac{1}{X_1\Omega^2}\frac{\mathrm{d}}{\mathrm{d}t}\right]u = \frac{-1}{X_1\Omega^2}\frac{\mathrm{d}u^+}{\mathrm{d}t}$$

This in fact is what Tam and Auriault[18] proposed for the reflection of a single-frequency wave and is the reason the formulas in Ref. 15 are restricted to positive imaginary $\mathrm{Im}(Z)$. It is clear that the inclusion of $R_0$ ($>0$ for damped reflections) does not affect the stability of the preceding choices, but the inclusion of $R_2\omega^2$ would introduce a second-order system whose characteristic roots have different signs:

$$\omega_{1,2} = i\left[-X_1/2R_2 \pm \sqrt{(X_1/2R_2)^2 + (1 + R_0)/R_2}\right]$$

and is, thus, always unstable unless care is taken to filter the unwanted components. Thus, the formula proposed by Davis,[10] including the term $R_2\omega^2$ for the damping of low-frequency waves, could not have worked because of its instability. It is clear that when the entire right-half plane $\mathrm{Re}(Z) \geq 0$ must be considered, in general, the construction of stable schemes to be valid for a broad range of variations of $Z$ would be formidable.

## Direct Scheme for Wave Reflection

Impedance $Z$ is a simplified model for the specification of the domain-entering component (reflection) $\hat{u}^- = \hat{u} - \hat{p} = (1 - Z)\hat{u}$, which, at the right boundary, is related to the domain-exiting (incident) wave $u^+$ by

$$\hat{u}^- = \hat{W}(\omega)\hat{u}^+ \tag{5}$$

where $\hat{W}(\omega) = (1 - Z)/(1 + Z)$. The complex function $\hat{W}$ is indeed a direct measure of the magnitude of the reflection and its relative phase with the incident wave. It is well known that this bilinear mapping maps the right half-plane $\mathrm{Re}(Z) \geq 0$ analytically into the interior of the unit circle $|\hat{W}| \leq 1$ in the $\hat{W} = U + iV$ plane, ensuring that the reflection is not amplified. It is unfortunate that the impedance $Z$, instead of the equivalent and more direct $\hat{W}$, has been measured and used conventionally to characterize the reflection. Equation (5) itself is already a direct way to compute the reflection from the incident. A corresponding expansion yields

$$\hat{W}(\omega) = U + iV = U_0 + U_2\omega^2 + \cdots + i(V_1\omega + V_3\omega^3 + \cdots) \tag{6}$$

which is sufficient to approximate a smooth contour of $\hat{W}$ within the unit circle and has the direct time-domain equivalent boundary condition

$$u^- = \hat{W}\left(\frac{\mathrm{d}}{i\,\mathrm{d}t}\right)u^+ \tag{7}$$

Equation (7) is obtained by a direct exchange of $\omega$ in Eqs. (5) and (6) with $(\mathrm{d}/i\,\mathrm{d}t)$ as in operational mathematics. Unlike $(1 + Z)$ in Eq. (3) for solving $u$, function $\hat{W}$ operates directly on the known incident wave $u^+(t)$ and is bounded by one, its application creates no system instability, and its efficiency and accuracy depend only on the range of application and complexity of the contour $\hat{W}[Z(\omega)]$. Equation (7) is sufficient to define a boundary operator for a physical variable, for example, pressure at a right boundary:

$$p = \left[1 - \hat{W}\left(\frac{\mathrm{d}}{i\,\mathrm{d}t}\right)\right]\frac{u^+}{2}$$

For monochromatic waves at the fixed frequency $\Omega$, Eq. (7) is simply

$$u^- = U(\Omega)u^+ + \frac{V(\Omega)}{\Omega}\frac{\mathrm{d}u^+}{\mathrm{d}t} \tag{8}$$

Furthermore, if $\hat{W}(\omega)$ is extended and Fourier transformable with the corresponding transformed function $W(t)$, Eq. (7) is equivalent to the convolution process of

$$u^-(t) = \int_{-\infty}^{\infty} W(t - \tau)u^+(\tau)\,\mathrm{d}\tau \tag{9}$$

The behaviors of $W(t)$ depend on $Z(\omega)$, which, as primarily an experimental quantity, may not be an analytic function of $\omega$. Equation (9) could assume various forms depending on how $Z(\omega)$ is treated or assumed analytically. A suitable form of $Z$ should yield a desirable numerical implementation of Eq. (9), which is the analytic time-domain equivalent for the frequency-domain impedance condition. We will demonstrate their applicability and address their generality with examples.

## Numerical Examples

Let us first focus on single-frequency cases or a finite band of frequencies over which $Z(\omega)$ has been given experimentally. Equation (7) involves the temporal operator $\hat{W}$ and the incident wave $u^+(t)$, which can be defined by the method of characteristics and represented using one-sided stencils consistent with the boundary scheme used. For each boundary point $u^-(t)$ is computed by updating $K + 1$ backward values of $u^+(t - k\Delta t)$, $0 \leq k \leq K$ ($\Delta t$ is the time step), and multiplying them with the difference operator $\hat{W}$ constructed by, for example, differentiation of $K$th-order Lagrange interpolants $\mathrm{L}_k$, that is,

$$u^-(t) = \sum_{k=0}^{K}(\hat{W}\mathrm{L}_k)u^+(t - k\Delta t)$$

Because one-sided difference operators are used, the order is chosen to provide accuracy of the highest derivative comparable to that of the scheme. To be consistent with the fourth-order inner scheme, we used six (five are necessary) plus the order of the highest derivative, or $K = 7$ if only the first derivative is needed. Figure 1 shows values of $R$ and $X$ (nondimensionalized by the free air impedance $\rho C$) measured and given in Motsinger and Kraft[20] for a 6.7% perforate acoustic treatment panel and of the recent mean least square fitted curves (dashed lines) by Tam and Auriault.[18] The corresponding $U$ and $V$ from the measured values (solid and open dots, respectively), from the fitted curves by Tam and Auriault[18] (dashed lines), and the seven-parameter expansions (solid lines):

$$U(\omega) = -1.1877 + 0.8918\omega^2 - 0.1349\omega^4 + 0.005916\omega^6 \quad (10a)$$

$$V(\omega) = 1.074\omega - 0.2921\omega^3 + 0.01586\omega^5 \quad (10b)$$

in $\omega$ (kHz) are shown in Fig. 2. For the case considered, the variation of resistance with frequency is not significant, and, hence, can be assumed constant as considered by Tam and Auriault.[18] Had higher-order approximants for $R$ and $X$ been used in Tam and Auriault's approach, the corresponding temporal operators would, in general, be unstable.

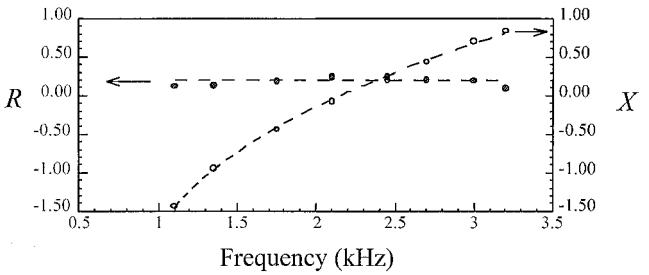


**Fig. 1 Measured[20] (● and ○, respectively) and fitted[18] (– – –) frequency-dependent resistance $R$ and reactance $X$ of a 6.7% perforate treatment panel at low sound intensity (no flow).**

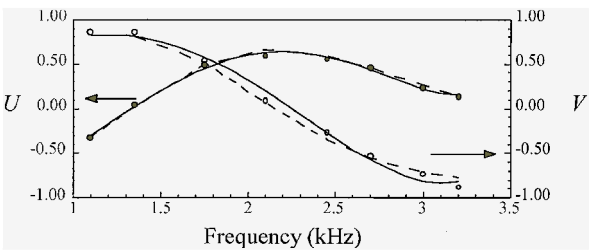


**Fig. 2 Approximated [——, based on Eq. (10); – – –, Tam and Auriault[18]] and measured[20] (● and ○, respectively) $U$ and $V$.**

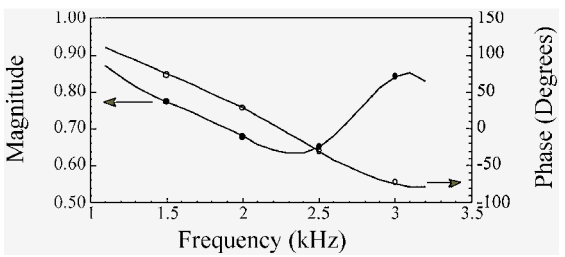


**Fig. 3 Computed magnitude and phase (● and ○, respectively) of the reflected wave at $x = 0$ using Eqs. (7) and (10) for four frequencies within the range of available data represented by Eq. (10) (——).**

Consider at $x = 0$ the reflection of the incident wave, $u^+ = 2\cos\Omega(x - t)$. Figure 3 compares the magnitude and phase of Eq. (10) (solid lines) with those (open and solid dots, respectively) of the computed time-domain reflection at $x = 0$ using a seven-point backward Lagrange approximant of Eqs. (7) and (10) for four frequencies spanning the range of application $1.1 \leq \omega \leq 3.2$ kHz of the impedance data. Both magnitude and phase are well represented. Figure 4 compares the pressure envelopes of the exact solution with fitted impedance according to Eq. (10) (dashed line), the exact solution with measured impedance at $\omega = 3.0$ kHz (diamonds), and the time-domain solution (solid line) computed using Eqs. (7) and (10) and the compact third-order nonuniform scheme (C3N) of Fung et al.[14] on a uniformly spaced 151 grid having at least seven points per wavelength for frequencies up to 4.0 kHz. The computed reflection at $x = 0$ using Eqs. (7) and (10) over a period of time corresponding to a physical domain traveled of 1.8 m or between $[-150, 0]$ is phase and magnitude accurate, and the minor differences in the fitted and measured impedance values are within the error of approximation, which can be improved by increasing the order of approximation for Eq. (7). Figure 5 shows the application of Eqs. (7) and (10) to the reflection of a harmonic-Gaussian pulse defined at $t = 0$, following Tam and Auriault[18] as

$$u(x, 0) = 0$$

$$p(x, 0) = \exp[-0.0044(x + 83.333)^2]\cos[0.444(x + 83.333)]$$

The initial pressure pulse is centered at 2.0 kHz and has a spectrum half-width of 0.5 kHz. The computed solution (solid line) at $t = 150$ accurately matches the exact frequency-domain solution.

To assess further the applicability of the present approach, the values of resistance and reactance, shown in Fig. 6, measured at the highest pressure level for the same perforate, were selected.[20]

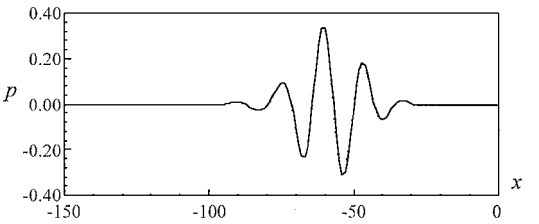


**Fig. 5 Reflected pressure pulses at $t = 150$: ——, time-domain solution, and · · ·, exact solution.**

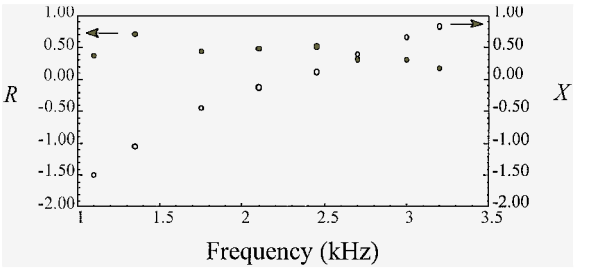


**Fig. 6 Resistance (●) and reactance (○) of a 6.7% perforate treatment panel measured at the highest sound intensity from top lines of Table 1 of Ref. 20.**

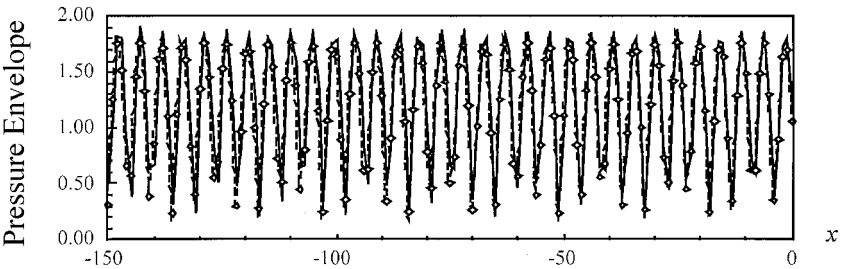


**Fig. 4 Pressure envelopes at a frequency of 3.0 kHz: ——, time-domain solution; – – –, exact solution based on Eq. (10); and ◇, exact solution based on measured impedance.**

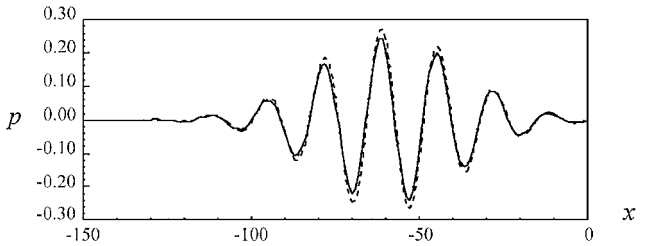


**Fig. 7 Reflected pressure pulses at $t = 150$: ——, time-domain solution; · · ·, exact solution based on Eq. (11); and – – –, exact solution based on constant resistance for impedance measured at the highest sound intensity given in Ref. 20.**

The variation in resistance is substantial, and it is not immediately apparent how the schemes proposed in Ref. 18 can be extended to include it. Here, the equations

$$U(\omega) = -0.9196 + 0.5707\omega^2 - 0.07742\omega^4 + 0.003112\omega^6 \tag{11a}$$

$$V(\omega) = 0.7511\omega - 0.1906\omega^3 + 0.009163\omega^5 \tag{11b}$$

($\omega$ measured in kilohertz) represent least-squares fits for the data in Fig. 6. A different initial harmonic-Gaussian pulse

$$u(x, 0) = 0$$

$$p(x, 0) = \exp[-0.0011(x + 83.333)^2]\cos[0.377(x + 83.333)]$$

centered at 1.7 kHz, having a spectrum half-width of 0.275 kHz, is chosen for the assessment. Figure 7 compares, at $t = 150$, the computed pressure pulse (solid line), the exact solution (dotted line), and the exact solution based on the assumption of constant mean resistance (dashed line).

Although the computed pulse is accurately predicted, the inadequacy in the assumed constant resistance of $R = 0.41$ amounts to a visible phase shift in the underdamped reflection. No algorithmic changes are needed in the present approach for different impedance data.

## Broadband Reflection

Equation (10), or any finite expansion of Eq. (6) in the form of an algebraic series, cannot generally satisfy the requirement that the reflected waves must not be amplified, $|\hat{W}| < 1$, over the entire frequency range of $0 \leq \omega < \infty$, or at least the range of the existing, physical, or spurious, waves in a computation. The behaviors of $W(t)$ must be explored for some model of $Z$, which primarily is an experimental quantity. There have been various models proposed for various types of impedances. The simple model used by Tam and Auriault[18] to represent the data in Fig. 1 is suitable for the present discussion:

$$Z(\omega) = R_0 + i(X_{-1}/\omega + X_1\omega) \tag{12}$$

where $R_0$, $X_{-1}$, and $X_1$ are given as 0.2, −13.48, and 0.0739, respectively, when $\omega$ is measured in kiloradians/second, or, equivalently, $R_0 = 0.2$, $X_{-1} = -0.1982$, and $X_1 = 5.0252$ for nondimensional $\omega$. Now $Z$ has been extended to the entire complex frequency plane, with the only restriction that $R_0 > 0$. Given a data set over a finite range of $\omega$, there could be other, more suitable, choices. However, the simple algebraic form of Eq. (12) yields the simple poles of $\hat{W}$:

$$\omega_{1,2} = \pm\omega_R + i\omega_I, \qquad \omega_R = \sqrt{(-X_{-1}/X_1) - [(1 + R_0)/2X_1]^2}$$

$$\omega_I = (1 + R_0)/2X_1 \tag{13}$$

both of which lie in the upper complex plane $\mathrm{Im}(\omega_j) > 0$, $j = 1, 2$, if $X_1 > 0$ and $X_{-1} < 0$. This implies that $W(t)$ is causal:

$$W(t) = \begin{cases} \mathrm{i}\sum_{j=1}^{2} \mathrm{residue}[\hat{W}(\omega)e^{i\omega t}, \omega_j], & t \geq 0 \\ 0, & t < 0 \end{cases}$$

$$u^-(t) = \int_{-\infty}^{t} W(t - \tau)u^+(\tau)\,\mathrm{d}\tau \tag{14}$$

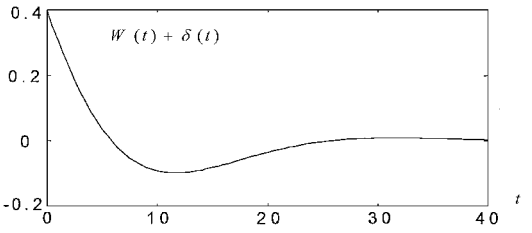


**Fig. 8 Reflection kernel.**

or only the history of $u^+(\tau)$ up to the current time $t$ determines the reflection, and the exponential decay determines the extent to which the history of $u^+(\tau)$ be recorded. For the values in Eq. (12), $W(t)$ has the form

$$W(t) = [2H(t)/X_1][\cos\omega_R t - (\omega_I/\omega_R)\sin\omega_R t]e^{-\omega_I t} - \delta(t) \tag{15}$$

where $H(t)$ is the Heaviside function and $\delta(t)$ the Dirac delta function. Figure 8 plots $W(t) + \delta(t)$ for $0 < t < 40$. Beyond this range, $W(t) + \delta(t)$ is either zero, when $t < 0$, or insignificantly small $|W(t) + \delta(t)| < 0.002$. Equation (15) implies not only the feasibility but also the practicality of enforcing a full spectrum of wall reflectivity with a finite time history of $T \sim 40$ dimensionless units (equivalent to 40 grid points traveled). This history $T$ for the model of Eq. (12) is inversely proportional to $\omega_I$, the imaginary part of the poles of $\hat{W}$. A shorter $T$ corresponds to a more compact implementation of Eq. (14). Unlike that of the differential operators in Eqs. (7) and (8), the implementation of the integral Eq. (14) is rather insensitive to numerical error. This opens up the prospect of finding equivalent compact, unconditionally stable integral operators for short-range applications.

A straightforward implementation of Eq. (14) requires the integral sum

$$u^-(t) = \sum_{k=0}^{T/\Delta t} W(k\Delta t)u^+(t - k\Delta t)$$

and correspondingly a large amount of storage of $T/\Delta t$ ($40/0.25 \sim 160$) points, compared to the substantially lower storage of $K = 11$ in the approximation of Eq. (10). However, because $u^+(x, t)$ has the characteristic form $u^+(x - t)$ the implication is that Eq. (14) can be reformulated at boundary $x_b$ as

$$u^-(x_b, t) = \int_{x_b}^{x_b + T} W(x - x_b)u^+(x, t)\,\mathrm{d}x \tag{16}$$

which requires only $T/\Delta x$ (40 additional $x$ storage points in this case). Equation (16) is preferred over Eq. (14) for the savings of $\Delta x/\Delta t$ in computer storage. However, the spatial implementation would complicate the otherwise simple data flow whenever irregular boundaries are encountered, whereas Eq. (14) preserves a space–time independent data structure.

All of the preceding numerical experiments have been repeated using both alternatives, Eqs. (14) and (16). The results are independent of implementation over the frequency range of the measured data. The differential approach, however, has encountered various numerical problems when extended to larger domains, longer computation time, or broader ranges of frequency. They are the round-off problem with smaller time steps, the amplification of spurious waves that have high-frequency contents, and thus inapplicability beyond the frequency range. These numerical problems can be mitigated using digital filters or smoother data representations for the higher derivatives at the expense of increased data processing time and storage. The range limitation has been solved by extensions such as Eq. (12), which may assume other advantageous forms. Further exploration of these extensions is beyond the scope of the present study.

## Broadband Plane Reflection

There have been quite a number of analytical solutions designed for benchmarking and validating time-domain numerical schemes for computational aeroacoustics (CAA).[21,22] However, none of these problems has involved a soft impedance wall. There seems to be a lack of reference literature on the transient solution of waves bounded by an impedance plane. The classical solution of the spherical harmonic point source above an impedance plane is well known for its fundamental importance in field and in situ impedance measurements, but its integral form is notoriously difficult for computation with general impedance values.[3] The difficulties arise from the varying incident angles from the source to the points of reflection and the necessary but ineffective conversion into plane waves before the application of the impedance condition. To verify our approach for general broadband multidimensional applications, a compact transient solution in two dimensions is warranted. The reflection of a two-dimensional Gaussian pulse from a solid wall using the superposition of an image pulse can be found in Ref. 21. When this method is used in problems with impedance walls, the solution we found (see Appendix) cannot satisfy an arbitrary initial field, but is useful for numerical validation. The analytical solution structure of the reflection of an initially Gaussian-like pulse is quite complicated due to the definition of impedance in the frequency domain, and its numerical evaluation is very time-consuming compared to the present discrete method (see Appendix).

Figure 9 shows the initial pressure contours of a Gaussian-like pulse, Eq. (A12) in the Appendix, with the impedance wall of Eq. (12) at $y = -32$. The fingertip shapes around the pulse are due to the analytic continuation of the initial spatial pressure distribution into the negative time in the solution process. These shapes disappear as the impedance approaches that of a solid wall and the initial pulse approaches the benchmarking Gaussian pulse given in Ref. 21. Figure 10a shows the computed pressure contours of this pulse at $t = 32$ using the implicit C3N scheme and decoupled formulation of Fung et al.[14] This formulation allows the reduction of the multidimensional Euler equation into a system of one-dimensional equations, and the application of boundary condition is, thus, the same as the one-dimensional case. Unlike the plane wave theory in frequency domain, there is no need to identify the incident wave angle before the application of impedance. Here Eqs. (14) and (16) are applied to the normal wall-bound wave component $u_n + p$ to compute the domain-entering reflection $u_n - p$, and $u_n$ is simply the vertical velocity component $v$. Each grid unit is 5 mm, corresponding to the effective frequency range of the pulse from 0 Hz up to 3.6 kHz. Both implementations, Eqs. (14) and (16), have rendered the same result as the analytical solution plotted in Fig. 10b. Figures 11a and 11b give the computed and analytical contours, respectively, at $t = 64$ when the fronts of the pulse reach the numerical boundaries. Figures 12a and 12b compare the computed wall pressure (solid lines) with the analytic values (dashed lines) at the respective $t = 32$ and 64, again showing excellent agreement. The additional dotted lines are the computed pressure for an initially Gaussian pressure pulse, with $u(x, y, 0) = v(x, y, 0) = 0$, which corresponds to no analytic solution known to the authors.

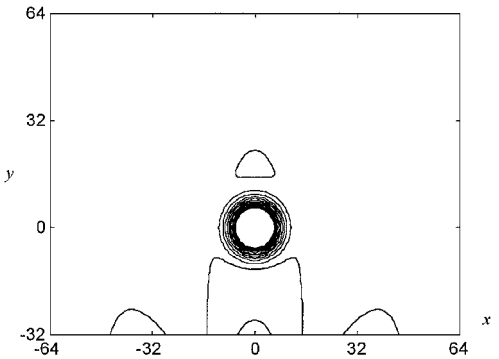


**Fig. 9 Initial pressure contours of a Gaussian-like pulse (contour levels: − 0.105 + increments of 0.03).**

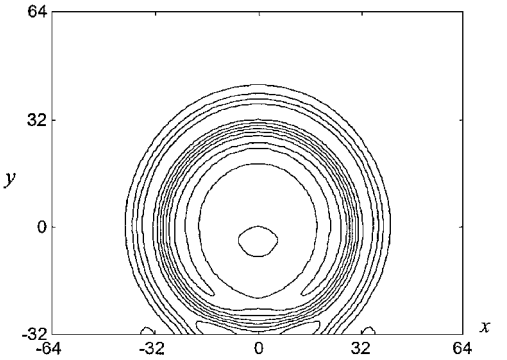


**Fig. 10a Computed pressure contours at $t = 32$ (contour levels: − 0.105 + increments of 0.03).**

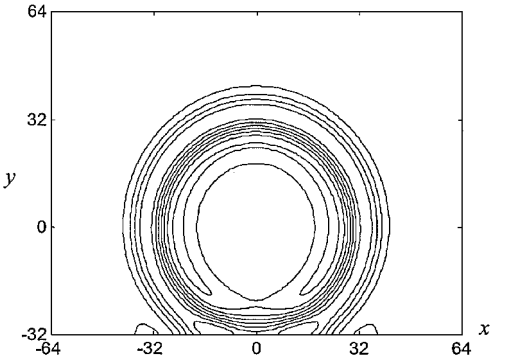


**Fig. 10b Analytical pressure contours at $t = 32$ (contour levels: − 0.105 + increments of 0.03).**

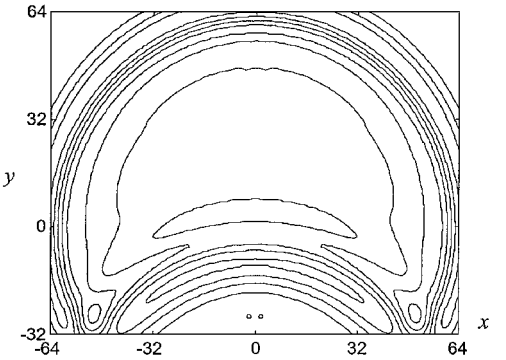


**Fig. 11a Computed pressure contours at $t = 64$ (contour levels: − 0.105 + increments of 0.03).**

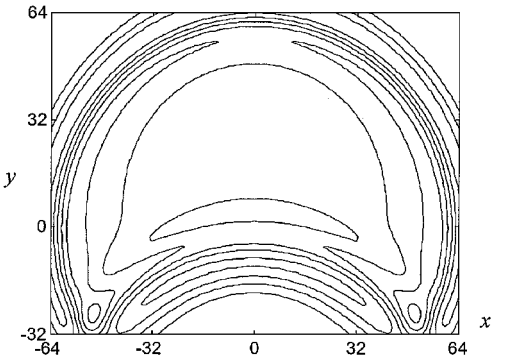


**Fig. 11b Analytical pressure contours at $t = 64$ (contour levels: − 0.105 + increments of 0.03).**

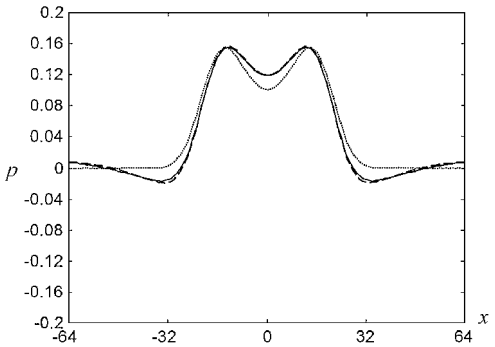


**Fig. 12a Wall pressure distributions at $t = 32$ for ——, calculation of modified Gaussian pulse equation (A12); – – –, analytical solution of modified Gaussian pulse equation (A12); and · · ·, calculation of a pure Gaussian pulse.**

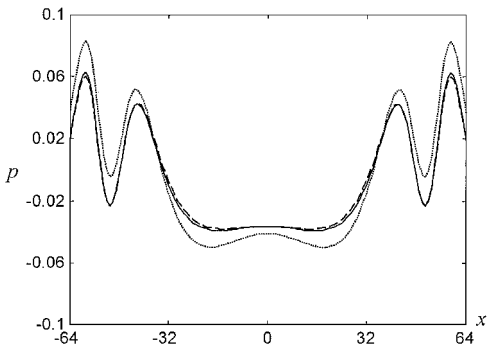


**Fig. 12b Wall pressure distributions at $t = 64$ for ——, calculation of modified Gaussian pulse equation (A12); – – –, analytical solution of modified Gaussian pulse equation (A12); and · · ·, calculation of a pure Gaussian pulse.**

## Further Extensions

In the presence of a mean flow over a reflective surface characterized by the impedance $Z$, continuity of particle displacement normal to the surface leads to the boundary condition[23] (right wall assumed here)

$$\hat{u}_n = (\hat{p}/Z) + (1/i\omega)\boldsymbol{M}_0 \cdot \nabla(\hat{p}/Z) - (\hat{p}/i\omega Z)\boldsymbol{n} \cdot (\boldsymbol{n} \cdot \nabla \boldsymbol{M}_0) \quad (17)$$

where $\boldsymbol{n}$ is the unit normal vector directed into the fluid, $\boldsymbol{M}_0$ mean Mach number vector, and $Z$ is ordinarily defined and measured at the zero mean flow condition. For mean flows satisfying the Navier–Stokes equations and the nonslip wall condition, $\boldsymbol{M}_0 = 0$, Eq. (17) reduces to $\hat{u}_n = \hat{p}/Z$, and the same time-domain extensions given here apply. In most applications when the details at the wall, including the boundary layer and its reactions to disturbances, are not of immediate concern, the Euler equations are preferred. Assuming the mean flow of $M_0$ is tangent to the plane surface in the $y$ direction, Eq. (17) reduces to

$$\hat{u}_n = \frac{\hat{p}}{Z} + \frac{M_0}{i\omega Z}\frac{\partial \hat{p}}{\partial y} \quad (18)$$

Tam and Auriault[18] explored the implementation of Eq. (18). Their analysis supported an instability of Kelvin–Helmholtz type. To avoid this instability of implementation, they suggested the replacement of Eq. (18) with $\hat{u}_n = \hat{p}/Z'$ and the modified impedance $Z'(M_0, \omega)$ to be determined experimentally. Özyörük et al.[19] implemented Eq. (18) in time domain successfully and found stable solutions in their numerical experiments, contradicting Tam and Auriault's analysis.

For plane harmonic waves, the convective derivative in Eq. (18) can be replaced by $-ik_y$ to yield an equivalent flow impedance $Z'(M_0, \omega)$ and boundary condition in the form

$$\hat{u}_n = \hat{p}/Z', \qquad Z' = Z/(1 - M_0/c_y), \qquad \text{where } c_y = \omega/k_y \quad (19)$$

which, indeed, had been proposed by Ingard[24] in 1959. When the phase speed $c_y(\omega)$ is known [for plane waves, $c_y(\omega)$ equals $\csc(\theta)$ of the incident angle $\theta$ and approaches unity at grazing angle $\theta = \pi/2$], Eq. (19), or in the form of Eq. (7), can then be applied to the acoustic modes $u_n \pm p$ of the Euler equations, in the same way as those of the acoustic/wave equation, to determine $u_n$ and $p$ at the boundary. In more complex situations where multiple reflections occur and knowledge of $c_y(\omega)$ is not available or easily approximated, a full implementation of Eq. (18) in time domain may assume the form

$$u_n^-(t) + \int_{-\infty}^{+\infty} W_{II}(t-\tau)\frac{\partial}{\partial y}u_n^-(\tau)\,\mathrm{d}\tau = \int_{-\infty}^{+\infty}\left[W_I(t-\tau) + W_{II}(t-\tau)\frac{\partial}{\partial y}\right]u_n^+(\tau)\,\mathrm{d}\tau \quad (20)$$

where $W_I$ and $W_{II}$ are inverse Fourier transforms of $\hat{W}_I(\omega) = (1-Z)/(1+Z)$ and $\hat{W}_{II}(\omega) = [M_0/i\omega(1+Z)]$, respectively. Implementation of Eq. (20) should, in principle, be equivalent to Eq. (19) for plane harmonic waves and, therefore, mathematically stable. Note, however, that the validity of Eq. (18) would imply that the additional pressure change was purely kinematic, due entirely to convection or the Eulerian transformation, and the presence of a flow was assumed not to alter the material impedance characteristics $Z(\omega)$. Because convective effects are timelike, to establish this assumption itself requires an extensive comparison of experiment and time-domain reflection theory. The use of Eq. (20) is not recommended until the difference between Eqs. (18) and (19) is firmly and experimentally established.

It was mentioned earlier that implementation of time-domain impedance condition is straightforward for the dimensionally split and decoupled system[14] of the linearized isentropic Euler equations. For the full multidimensional Euler equations, a general-purpose computational fluid dynamics/CAA code would cast the equations at a boundary surface $x = \text{const}$ in the form

$$\frac{\partial u_i}{\partial t} + \lambda_i \frac{\partial u_i}{\partial x} + a_{ij}\frac{\partial u_j}{\partial y} = 0$$

where $u_i$ are the $x$-directional characteristic variables, $\lambda_i$ are their corresponding eigenvalues, and $a_{ij}$ is the $y$-Jacobian matrix transformed by the normalizing $x$-directional eigenvector matrix; compare Eq. (6.163–6.165), p. 405, of Ref. 25. These Riemann invariants are coordinate independent, or $(x, y)$ can be viewed as generalized curvilinear coordinates $(\xi, \eta)$ with the straightforward extension to the third dimension in the $x = \text{const}$ boundary surface. The acoustic modes of the characteristic variables corresponding to the eigenvalues $M_x \pm 1$ are to be coupled in a similar way as Eq. (18) or Eq. (20). Indeed, as pointed out earlier, a proper choice of $Z$ covers most admissible boundary conditions for the Euler equations, and those of the Navier–Stokes as well, except for the direct constraints on the tangential components such as nonslip wall conditions. The actual implementation for different schemes, or different types of $Z$, would depend on other considerations such as solution efficiency and is beyond the scope of the present investigation. The present work generalizes the concept of impedance to allow broader choices of $Z$ for implementation of robust numerical and physical boundary conditions.

## Conclusion

It is shown that the complex reflection coefficient $\hat{W}(Z)$ corresponds to a stable, bounded system for wave reflection at a boundary, whereas a direct translation of impedance $Z(\omega)$ corresponds in general to an unstable system. Direct construction of time-domain reflection condition from an expansion of $\hat{W}(Z)$ leads to numerically stable, accurate, and easily implementable schemes for waves. The concept of impedance has been extended analytically to an equivalent kernel of reflection. It is shown and demonstrated that the algebraic type of impedance model corresponds to pulselike kernels and compact integral formulas for full-range implementations of time-domain impedance conditions. The agreement with an

analytic solution derived here is excellent, substantiating the validity of the present approach and the accuracy of the proposed implementations. The theory proposed enables the direct solution of initial boundary value problems, which is advantageous in making direct comparisons with experiments.

## Appendix: Analytical Pulses at Plane Impedance Wall

The velocity potential $\phi$ of a localized pressure disturbance incited at $t = 0$ satisfies the wave equation and the initial and boundary conditions [with the same reference quantities as in Eq. (1)]

$$\frac{\partial^2\phi}{\partial t^2} - \left(\frac{\partial^2\phi}{\partial x^2} + \frac{\partial^2\phi}{\partial y^2}\right) = 0 \tag{A1}$$

$$t = 0: \qquad \phi = 0, \qquad \frac{\partial\phi}{\partial t} = g[r(x, y)] \tag{A2}$$

$$y = 0: \qquad \hat{p} = Z(\omega)\hat{v} \tag{A3}$$

where the sound pressure $p$ and velocity components $u$ and $v$ in the $x$ and $y$ directions, respectively, are related to derivatives of the potential:

$$u = \frac{\partial\phi}{\partial x}, \qquad v = \frac{\partial\phi}{\partial y}, \qquad p = -\frac{\partial\phi}{\partial t} \tag{A4}$$

The physical domain of interest is $x \in (-\infty, \infty)$, $y \in [0, \infty)$. The initial pulse has circular wave fronts about origin $(x_s, y_s)$ and distribution $g(r)$, where $r(x, y) = \sqrt{[(x - x_s)^2 + (y - y_s)^2]}$. Here we consider the Gaussian distribution

$$g[r(x, y)] = -e^{-\ln 2(r/B)^2} \tag{A5}$$

The solution $\phi(x, y, t)$ can be expressed linearly as the sum of the incoming waves $\phi_{\text{in}}(x, y, t)$ and reflected waves $\phi_{\text{ref}}(x, y, t)$: $\phi(x, y, t) = \phi_{\text{in}}(x, y, t) + \phi_{\text{ref}}(x, y, t)$. Using the Hankel transform and denoting its components with ˜, the incoming waves $\phi_{\text{in}}(x, y, t)$ due to the source $g(r)$ can be expressed as

$$\phi_{\text{in}}(x, y, t) = \int_0^\infty \tilde{g}(k_r) J_0[k_r r(x, y)] \sin(k_r t)\, \mathrm{d}k_r, \qquad \text{for } t \geq 0 \tag{A6}$$

Here

$$\tilde{g}(k_r) = \int_0^\infty r g(r) J_0(k_r r)\, \mathrm{d}r$$

where $k_r$ is the Hankel transform parameter and $J_0$ the zero-order Bessel function. When the wave number parameter $k_r$ is renamed $\omega$, making the odd extension of $\tilde{g}(\omega)$ for negative $\omega$, the Hankel transform in Eq. (A6) assumes the form of a Fourier transform in $\omega$, that is,

$$\phi_{\text{in}}(x, y, t) = \frac{1}{2i}\int_{-\infty}^{\infty} \text{sign}(\omega)\tilde{g}(\omega) J_0[\omega r(x, y)] e^{i\omega t}\, \mathrm{d}\omega \tag{A7}$$

To apply the conventional impedance defined for plane waves, the cylindrical waves just described need to be converted into plane wave components. With $x_s = 0$ for simplicity, $J_0$ assumes the convenient Fourier cosine transform form[26]

$$J_0[\omega r(x, y_s)] = J_0(\omega|x|) = J_0(|\omega|x) = \frac{2}{\pi}\int_0^{|\omega|} \frac{1}{k_y}\cos(k_x x)\, \mathrm{d}k_x$$

$$= \frac{1}{\pi}\int_{-|\omega|}^{|\omega|} \frac{1}{k_y} e^{-ik_x x}\, \mathrm{d}k_x$$

and[27]

$$J_0\left[\omega\sqrt{x^2 + (y - y_s^2)}\right]$$

$$= \frac{1}{\pi}\int_{-|\omega|}^{|\omega|} \frac{1}{k_y}\exp[-i(k_x x + k_y|y - y_s|)]\, \mathrm{d}k_x$$

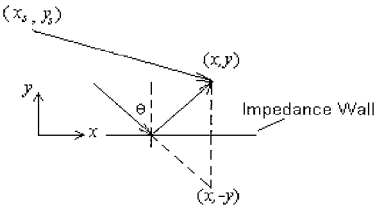


**Fig. A1 Wave reflection off impedance wall.**

where $k_y = \sqrt{(\omega^2 - k_x^2)}$. Thus, the incoming plane waves are

$$\phi_{\text{in}}(x, y, t) = \frac{1}{2\pi i}\int_{-\infty}^{\infty} \text{sign}(\omega)\tilde{g}(\omega)$$

$$\times \int_{-|\omega|}^{|\omega|} \frac{1}{k_y}\exp[-i(k_x x + k_y|y - y_s| - \omega t)]\, \mathrm{d}k_x\, \mathrm{d}\omega \tag{A8}$$

According to the law of plane wave reflection, each reflected wave component coming to the image point $(x, -y)$ is modified by the amplitude $|C_r|$ and phase shift $\beta$ (Fig. A1). The corresponding reflected waves are

$$\phi_{\text{ref}}(x, y, t) = \frac{1}{2\pi i}\int_{-\infty}^{\infty} \text{sign}(\omega)\tilde{g}(\omega)$$

$$\times \int_{-|\omega|}^{|\omega|} |C_r|\frac{1}{k_y}\exp\{-i[k_x x + k_y(y + y_s) - \omega t + \beta]\}\, \mathrm{d}k_x\, \mathrm{d}\omega$$

$$= \frac{1}{\pi}\int_0^\infty \tilde{g}(\omega)\sin(\omega t)$$

$$\times \int_{-|\omega|}^{|\omega|} |C_r|\frac{1}{k_y}\exp\{-i[k_x x + k_y(y + y_s) + \beta]\}\, \mathrm{d}k_x\, \mathrm{d}\omega$$

in which $C_r$ is the reflection coefficient

$$C_r = \frac{1 - Z\cos\theta}{1 + Z\cos\theta} = |C_r(\omega, k_x)|\exp[-i\beta(\omega, k_x)]$$

where $\theta = \sin^{-1}(k_x / k_0)$, $k_0 = \omega$.

By taking the real part, one obtains the reflected waves:

$$\phi_{\text{ref}}(x, y, t) = \int_0^\infty \tilde{g}(\omega) R(\omega)\sin(\omega t)\, \mathrm{d}\omega \tag{A9}$$

where

$$R(\omega) = \frac{1}{\pi}\int_{-|\omega|}^{|\omega|} |C_r|\frac{1}{k_y}\cos[k_x x + k_y(y + y_s) + \beta]\, \mathrm{d}k_x$$

$$= \frac{2}{\pi}\int_0^{|\omega|} |C_r|\frac{1}{k_y}\cos[k_y(y + y_s) + \beta]\cos(k_x x)\, \mathrm{d}k_x$$

The combined velocity potential takes the form

$$\phi(x, y, t) = \int_0^\infty \tilde{g}(\omega)\{J_0[\omega r(x, y)] + R(\omega)\}\sin(\omega t)\, \mathrm{d}\omega \tag{A10}$$

or the acoustic pressure is

$$p(x, y, t) = -\frac{\partial\phi}{\partial t}$$

$$= -\int_0^\infty \omega\tilde{g}(\omega)\{J_0[\omega r(x, y)] + R(\omega)\}\cos(\omega t)\, \mathrm{d}\omega \tag{A11}$$

When $|C_r| \to 1$, $\beta \to 0$,

$$R(\omega) \to J_0\left[\omega\sqrt{x^2 + (y + y_s)^2}\right] = J_0[\omega r(x, -y)]$$

the solution returns to that with a solid wall.

In the final solution, only the velocity field [Eq. (A10)] satisfies the initial condition $\phi = 0$, the pressure field [Eq. (A11)] is no longer

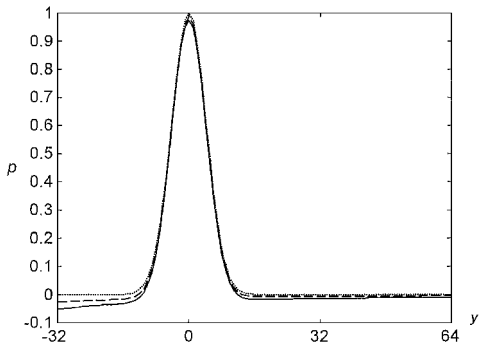


**Fig. A2 Initial pressures at $x = 0$ for ——, modified Gaussian equation (A12); – – –, modified Gaussian equation (A13); and · · ·, pure Gaussian.**

the same as the intended primary one $(\partial\phi/\partial t) = g(r)$ but is changed to the modified form

$$\frac{\partial \phi}{\partial t} = g(r) + \int_0^\infty \omega \tilde{g}(\omega) R(\omega)\, \mathrm{d}\omega \tag{A12}$$

due to the odd extension of $\tilde{g}(\omega)$ to obtain Eq. (A7). If instead the Heaviside function $H(t)$ is introduced into the incoming potential for extension:

$$\phi_{\text{in}}(x, y, t) = \int_0^\infty \tilde{g}(k_r) J_0[k_r r(x, y)] H(t) \sin(k_r t)\, \mathrm{d}k_r \qquad t \in (-\infty, \infty)$$

the corresponding total potential becomes

$$\phi(x, y, t) = \int_0^\infty \tilde{g}(\omega) \left[ J_0[\omega r(x, y)] + \frac{1}{2} R(\omega) \right] \sin(\omega t)\, \mathrm{d}\omega + \frac{1}{\pi^2} \int_0^\infty \int_0^\infty \int_{-k_r}^{k_r} |C_r| \tilde{g}(k_r) \frac{1}{k_p} \frac{k_r}{k_r^2 - \omega^2} \times \cos[k_x x + k_p(y + y_s) + \beta] \cos(\omega t)\, \mathrm{d}k_x\, \mathrm{d}\omega\, \mathrm{d}k_r \tag{A13}$$

where $k_p = \sqrt{(k_r^2 - k_x^2)}$.

Figure A2 compares the initial pressure distributions of the modified pulses, Eq. (A12) (solid line) and Eq. (A13) (dashed line), with the unmodified Gaussian pulse (dotted line) of half-pulse width, $B = 5$, at the line of symmetry, $x = 0$. The pulse given by Eq. (A13) is indeed closer to a Gaussian pulse than that of Eq. (A12), but the corresponding velocity field is nonzero at $t = 0$. The continuation into the negative time introduces a corresponding reflection seen at $t = 0$. It can be verified that the farther away the initial pulses are from the wall or the stronger the absorption (high frequencies), the closer the initial pulse is to a Gaussian one. The analytical solution for an initially Gaussian pressure pulse with zero velocity has not been found by the authors, nor has an analytic method for the general solution of Eqs. (A1–A3). The present time-domain approach with a causal extension of $W(t)$, however, can take on any initial set of $u$, $v$, and $p$ and solve the true initial boundary value problem.

The 20th-order Gaussian quadrature was used to numerically integrate Eq. (A11), and the Gauss–Chebyshev rule was used to evaluate $R(\omega)$ in which the weights and points are expressed in the closed analytical form

$$\int_{-1}^{1} \frac{f(s)}{\pi \sqrt{1 - s^2}}\, \mathrm{d}s \approx \frac{1}{n} \sum_{k=1}^{n} f\left[ \cos \frac{(2k - 1)\pi}{2n} \right]$$

where $f(s) = |C_r| \cos[(y + y_s)\omega\sqrt{(1 - s^2)} + \beta] \cos(\omega s x)$. The numerical integration of Eq. (A11) takes approximately $(875 \times N_G \times N_{GC} + 550)(\sim 1.8 \times 10^6)$ floating point operations per point in space/time, where $N_G (= 20)$ is the order of Gauss quadrature and $N_{GC} (\sim 100)$ the number of Gauss–Chebyshev points, compared to the $(1.31 \times 42 \times \text{time}/\Delta t \sim 1.4 \times 10^4)$ operations per point in the discrete method. Whereas the analytical solution takes 1.15 h to evaluate on a SGI-O2 workstation, the numerical solution at $t = 64$ takes only 40 s.

## Acknowledgments

Financial support for the second author on Hong Kong Polytechnic University Grant G-YW23 and computer support on Hong Kong Polytechnic University Grant G-S 735 are acknowledged. Thanks are also due to Caizhong Li of Sichuan Union University, Quanlin Wei of Renmin University of China, and Omar Sekkat of the Swiss Federal Institute of Technology for their kind assistance and helpful discussions on the analytical solution.

## References

[1] Pierce, A. D., *Acoustics*, Acoustical Society of America, New York, 1991, pp. 107–108.

[2] Jones, M. G., and Stiede, P. E., "Comparison of Methods for Determining Specific Acoustic Impedance," *Journal of the Acoustical Society of America*, Vol. 101, No. 5, Pt. 1, 1997, pp. 2694–2704.

[3] Stinson, M. R., "A Note on the Use of an Approximate Formula to Predict Sound Fields Above an Impedance Plane Due to a Point Source," *Journal of the Acoustical Society of America*, Vol. 98, No. 3, 1995, pp. 1810–1812.

[4] Chien, C. F., and Soroka, W. W., "Sound Propagation Along an Impedance Plane," *Journal of Sound and Vibration*, Vol. 43, No. 1, 1975, pp. 9–20.

[5] Embleton, T. F. W., Piercy, J. E., and Olson, N., "Outdoor Sound Propagation over Ground of Finite Impedance," *Journal of the Acoustical Society of America*, Vol. 59, No. 2, 1976, pp. 267–277.

[6] Attenborough, K., Hayek, S. I., and Lawther, J. M., "Propagation of Sound Above a Porous Half-Space," *Journal of the Acoustical Society of America*, Vol. 68, No. 5, 1980, pp. 1493–1501.

[7] Allard, J. F., and Champoux, Y., "In-Situ Two-Microphone Technique for the Measurement of the Acoustic Surface Impedance of Materials," *Noise Control Engineering Journal*, Vol. 32, No. 1, 1989, pp. 15–23.

[8] Cramond, A. J., and Don, C. G., "Reflection of Impulses as a Method of Determining Acoustic Impedance," *Journal of the Acoustical Society of America*, Vol. 75, No. 2, 1984, pp. 382–389.

[9] Tamura, M., "Spatial Fourier-Transform Method for Measuring Reflection Coefficients at Oblique Incidence. I: Theory and Numerical Examples," *Journal of the Acoustical Society of America*, Vol. 88, No. 5, 1990, pp. 2259–2264.

[10] Davis, S., "Low-Dispersion Finite Difference Methods for Acoustic Waves in a Pipe," *Journal of the Acoustical Society of America*, Vol. 90, No. 5, 1991, pp. 2775–2781.

[11] Tam, C. K. W., and Webb, J. C., "Dispersion-Relation-Preserving Difference Schemes for Computational Acoustics," *Journal of Computational Physics*, Vol. 107, No. 2, 1993, pp. 262–281.

[12] Taflove, A., *Computational Electrodynamics: The Finite-Difference Time-Domain Methods*, Artech House, Boston, 1995.

[13] Hu, F. Q., Hussaini, M. Y., and Manthey, J. L., "Low-Dissipation and Low-Dispersion Runge–Kutta Schemes for Computational Acoustics," *Journal of Computational Physics*, Vol. 124, No. 1, 1996, pp. 171–191.

[14] Fung, K.-Y., Man, R. S., and Davis, S., "An Implicit High-Order Compact Algorithm for Computational Acoustics," *AIAA Journal*, Vol. 34, No. 10, 1996, pp. 2029–2037.

[15] Yee, K. S., Shlager, K., and Chang, A. H., "An Algorithm to Implement a Surface Impedance Boundary Condition for FDTD," *IEEE Transactions on Antennas and Propagation*, Vol. 40, No. 7, 1992, pp. 833–837.

[16] Lee, C. F., Shin, R. T., and Kong, J. A., "Time Domain Modeling of Impedance Boundary Condition," *IEEE Transactions on Microwave Theory and Techniques*, Vol. 40, No. 9, 1992, pp. 1847–1851.

[17] Fang, J., and Xeu, D., "Numerical Errors in the Computation of Impedances by FDTD Method and Ways to Eliminate Them," *IEEE Microwave and Guided Wave Letters*, Vol. 5, No. 1, 1995, pp. 6–8.

[18] Tam, C. K. W., and Auriault, L., "Time-Domain Impedance Boundary Conditions for Computational Acoustics," *AIAA Journal*, Vol. 34, No. 5, 1996, pp. 917–923.

[19] Özyörük, Y., Long, L. N., and Jones, M. G., "Time-Domain Numerical Simulation of a Flow-Impedance Tube," *Journal of Computational Physics*, Vol. 146, No. 1, 1998, pp. 29–57.

[20] Motsinger, R. E., and Kraft, R. E., "Design and Performance of Duct Acoustic Treatment," *Aeroacoustics of Flight Vehicles: Theory and Practice*, edited by H. H. Hubbard, NASA RP-1258, 1991, Chap. 14, Table 1, p. 184.

[21]Tam, C. K. W., "Benchmark Problems and Solutions," *ICASE/LaRC Workshop on Benchmark Problems in Computational Aeroacoustics (CAA)*, edited by J. C. Hardin, J. R. Ristorcelli, and C. K. W. Tam, NASA CP-3300, 1995, pp. 1–13.

[22]Tam, C. K. W., and Hardin, J. C. (eds.), *Second Computational Aeroacoustics (CAA) Workshop on Benchmark Problems*, NASA CP-3352, 1997, pp. 1–44.

[23]Myers, M. K., "On the Acoustic Boundary Condition in the Presence of Flow," *Journal of Sound and Vibration*, Vol. 71, No. 3, 1980, pp. 429–434.

[24]Ingard, U., "Influence of Fluid Motion Past a Plane Boundary on Sound Reflection, Absorption, and Transmission," *Journal of the Acoustical Society of America*, Vol. 31, No. 7, 1959, pp. 1035, 1036.

[25]Tannehill, J. C., Anderson, D. A., and Pletcher, H. P., *Computational Fluid Mechanics and Heat Transfer*, Taylor and Francis, Washington, DC, 1997, p. 405.

[26]Oberhettinger, F., *Tables of Fourier Transforms and Fourier Transforms of Distributions*, Springer–Verlag, Berlin, 1990, p. 66.

[27]Brekhovskikh, L. M., *Waves in Layered Media*, Academic, New York, 1960, p. 239.

P. J. Morris
*Associate Editor*